processes

MDPI

Article

Study on the Fracture Propagation in Multi-Horizontal Well Hydraulic Fracturing

Qiquan Ran, Xin Zhou *, Jiaxin Dong, Mengya Xu, Dianxing Ren and Ruibo Li

Research Institute of Petroleum Exploration and Development, No. 20 Xueyuan Road, Haidian District, Beijing 100083, China; ranqq@petrochina.com.cn (Q.R.); djx1021@petrochina.com.cn (J.D.); xumengya@petrochina.com.cn (M.X.); rendianx@petrochina.com.cn (D.R.); liruibo01@petrochina.com.cn (R.L.)
* Correspondence: zhouxin510@petrochina.com.cn

Abstract: Multi-horizontal well hydraulic fracturing is a widely employed and highly effective method for stimulating tight and shale reservoirs. However, most existing studies primarily focus on investigating the impact of intra-well interference on fracture propagation while neglecting the influence of inter-well interference. Here, a multi-well hydraulic-fracture-propagation model is established to examine the effects of inter-well interference on fracture propagation within a multi-well system. In this study, based on the bilinear T-S criterion, the stiffness degradation is used to describe the damage and evolution process of fracture, the coupling process of fluid flow and solid damage and deformation is realized, and the dynamic distribution of inter-fracture flow is realized by using Kirchhoff function on the basis of the cohesive zone method (CZM) finite element model. Finally, the fracture-propagation model of multiple horizontal wells is established. Based on this model, the mechanism of inter-well interference on fracture propagation is studied, and the influence law of Young's modulus and fracture displacement on fracture propagation in multi-wells is investigated. The results show that the reservoir can be divided into self-influence area, tension area and compression area according to the stress distribution state in the hydraulic fracture propagation of multi-wells. The propagation rate of hydraulic fractures in horizontal wells is significantly accelerated when they propagate to the local tension area generated by the fracture tip of neighboring wells, and rapidly decreases as the hydraulic fractures continue to propagate to the compression area of neighboring wells. Rocks with a lower Young's modulus tend to be more plastic, forming hydraulic fractures with usually lower fracture lengths and usually larger fracture widths. The hydraulic fracture has an inhibitory effect on the propagation of fractures closer to each other in neighboring wells, and this inhibitory effect gradually increases as the distance decreases. The dominance of the dominant fracture to propagate in the self-influence area gradually decreases under inter-well and intra-well interference. As the dominant fracture propagates into the tension and compression areas of the neighboring well fractures, the feed fluid will show a brief rise and then eventually stabilize. This study quantifies the effect of inter-well interference on fracture propagation and lays the foundation for treatment optimization of small well spacing hydraulic fracturing.

Keywords: fracture propagation; inter-well interference; cohesive; hydraulic fracturing; numerical simulation

Citation: Ran, Q.; Zhou, X.; Dong, J.; Xu, M.; Ren, D.; Li, R. Study on the Fracture Propagation in Multi-Horizontal Well Hydraulic Fracturing. *Processes* **2023**, *11*, 1995. https://doi.org/10.3390/pr11071995

Academic Editor: Qingbang Meng

Received: 18 May 2023
Revised: 25 June 2023
Accepted: 27 June 2023
Published: 2 July 2023

1. Introduction

Tight reservoirs and shale reservoirs have gradually become the focus of oil and gas exploitation, and infill horizontal wells and small well spacing hydraulic fracturing technology can fully stimulate the reservoir and make underground crude oil efficiently used, which has now become the most important stimulation method for these reservoirs [1,2]. Previous studies have focused on the effect of intra-well interference on fracture propagation [3,4], but the effect of inter-well interference on fracture propagation has become particularly important in small spacing stimulation [5,6]. Since the small well spacing exploitation method is still

in its infancy, the mechanism and law of inter-well interference on fracture propagation are still unclear.

During hydraulic fracture propagation, the rock is damaged and fractures are formed under the injected high-pressure fluid. Currently, the majority of mathematical models employed for simulating fracture propagation rely on linear elasticity theory [7]. The drawbacks of those models are that they cannot accurately describe the fracture propagation process and their simulation results are severely controlled by the mesh shape [8]. In addition, these methods only discretize the body boundary, and this phenomenon can cause serious problems during iterative calculations. To address this phenomenon, a finite element method incorporating the CZM has been employed to simulate the propagation process of hydraulic fractures, taking into account the effects of propagation and softening at the fracture tip [9–11]. The finite element model based on CZM simulates the coupling process of incompressible viscous fluid and rock deformation, and the results show that the model is more accurate for describing the extension process of hydraulic fracturing [12]. In a related study, Guo et al. [13] utilized a novel CZM model that couples the flow-damage field to simulate the interaction between hydraulic fractures and natural fractures. Additionally, Li et al. [14] proposed an innovative cohesive unit for pore pressure, incorporating the Coulomb friction contact model to depict fracture contact behavior. Overall, the CZM-based finite element method exhibits considerable advantages over alternative approaches, as it encompasses fracture tip damage and evolution, rendering it good for modeling the fracture propagation.

To explore the impact of stress shadows and complex stress fields on fracture propagation, various methodologies, such as XFEM, BEM, FEM, UFM, and DEM, have been developed [15,16]. Notably, during the propagation of hydraulic fractures, pull-up damage arises at the fracture tip, leading to a reduction in stress within that particular region [17]. Lecampion et al. [18] conducted a study on fracture propagation in impermeable media using the extended finite element method (XFEM) and proposed the implementation of a specialized enrichment function at the fracture tip to capture pore size and pressure. However, this investigation did not account for the longitudinal fluid flow. In a different study, Chen et al. [19] examined fracture propagation in impermeable media by considering longitudinal flow and utilizing a cohesion law-controlled boundary element method (BEM). The obtained results displayed favorable agreement with field monitoring outcomes. Moreover, the opening of hydraulic fractures can cause compression of the surrounding reservoir, leading to alterations in pore pressure and stress fields adjacent to the fracture [20,21]. Sun et al. [22] employed the finite element method (FEM) to investigate hydraulic fracturing parameters in porous media, revealing a gradual decrease in fluid pressure within the fracture as the fracture length increases. Importantly, field diagnostic techniques have indicated that multiple fractures often propagate simultaneously, leading to uneven propagation due to the influence of stress shadows [23]. Subsequent researchers have highlighted that, in addition to stress shadowing, fracture propagation is also influenced by stress shadows, and perforation friction plays a crucial role in the dynamic distribution of flow [3,24]. However, the majority of existing studies have primarily focused on investigating intra-well interference of hydraulic fractures within a single well, with minimal consideration given to the dynamic distribution of fracturing fluid between fractures. In comparison to the aforementioned methods, the CZM offers notable advantages, including its robust node compilation capability, convenient coupling calculations, and fast computational speed. Consequently, CZM proves advantageous in terms of coupling dynamic flow distribution in this aspect.

To elucidate the behavior of fracture propagation in multi-horizontal well hydraulic fracturing, this study employs stiffness degradation to characterize the damage and evolution process of fractures based on the bilinear T-S criterion. Furthermore, it achieves the coupling of fluid flow and solid damage and deformation. By integrating the CZM finite element model, the dynamic distribution of flow in multiple fractures is realized through the application of Kirchhoff's law. Ultimately, a coupled model for fracture propagation

in multi-horizontal wells is established. Based on this model, the study investigates the mechanism of inter-well interference on fracture propagation, examining the impact of Young's modulus and fracture location on fracture propagation in multi-horizontal wells.

2. Mathematical Model

The core problem of the study on the interference of multi-fractures between wells on fracture propagation is to accurately describe the fracture propagation and the change of the stress field between wells. The CZM finite element method can accurately describe the damage and evolution of fractures, the tangential and normal flow of fracturing fluid in the fractures, the flow of fluid in porous media and the deformation of solids and has been widely used to describe the fracture initiation and propagation process during hydraulic fracturing.

2.1. Fluid Flow in the Fracture

The fracturing fluid opens the reservoir and forms a fracture at a pressure higher than the breakdown pressure. As shown in Figure 1, part of the fluid in the fracture flows tangentially along the heel to toe of the fracture, and the other part of the fluid leaks off along the wall of the reservoir under the pressure difference between the fracture and the matrix. For the tangential flow of fluid in the fracture, assuming that the fracturing fluid is an incompressible Newtown fluid, the overall volume balance equation for tangential flow established by Poiseuille is used in this study as follows [25].

$$q = -\frac{w^3}{12\mu}\nabla p \tag{1}$$

where q is the flow velocity of the flow along the fracture propagation direction, ∇p is the pressure difference of the flow along the fracture propagation direction, w is the fracture width in this cohesive unit and μ is the fracturing fluid viscosity.

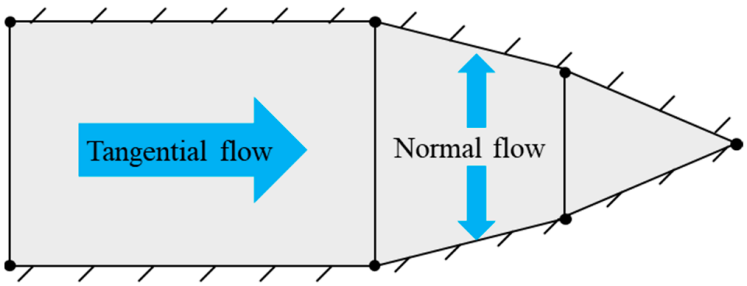

Figure 1. Flow patterns of fluids in the cohesive element.

To account for the leakage of fracturing fluid along the fracture wall, two permeable cohesive layers are introduced. These layers facilitate fluid leak-off along the fracture wall, as illustrated in Figure 2. The normal leak-off at the fracture surface can be characterized as follows:

$$\begin{cases} q_t = c_t\left(p_f - p_t\right) \\ q_b = c_b\left(p_f - p_b\right) \end{cases} \tag{2}$$

where p_t and p_b are the pore pressure in the top and bottom layer unit, respectively, p_f is the pressure of the cohesive unit, c_t and c_b are the leak-off coefficients at the top and bottom layers, respectively, and q_t and q_b are the normal volume leak-off rates at the top and bottom layers, respectively.

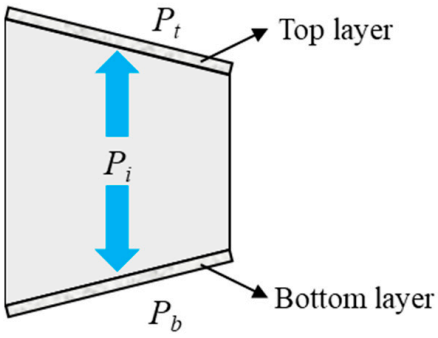

Figure 2. Normal flow for cohesive surface.

Considering the flow along the fracture surface in the fracture, the normal flow of the fluid perpendicular the fracture surface and the variation of the fracture width during the hydraulic fracturing, the continuity equation for fluid in the fracture can be expressed as:

$$\frac{\partial w}{\partial t} + \nabla \cdot q + (q_t + q_b) = Q(t)\delta(x, y) \tag{3}$$

where *Q(t)* is the fluid source for this unit.

2.2. Damage and Evolution of Fractures

The flow of fluid in the fracture at a macroscopic level, the flow of fluid in the porous medium at a microscopic level and the elastic deformation and damage of the rock are all interconnected. The CZM employs the traction-separation law to model the behavior of interfaces. In the model, Biot's effective stress principle is employed to describe the effective stress [26]. This principle considers the interaction between fluid flow and solid deformation, accounting for the impact of fluid pressure on the effective stress within the rock matrix. This principle considers the interaction between fluid flow and solid deformation, accounting for the impact of fluid pressure on the effective stress within the rock matrix.

$$\sigma_{ij} = \sigma'_{ij} + \alpha p \delta_{ij} \tag{4}$$

where $\sigma_{i,j}$ and $\delta'_{i,j}$ is the total stress and the effective stress, respectively, α is the Biot coefficient and $\delta_{i,j}$ is the tensor of Kronecker.

The damage model of the cohesive unit establishes the relationship between tensile stresses and displacements between adjacent meshes. V. Tomar et al. [27] proposed a bilinear T-S criterion, depicted in Figure 3, which comprises two components for damage evolution. The first component involves determining the relationship between the effective displacement, denoted as δ_m^f, at complete failure, relative to the effective displacement, δ_m^0 at the onset of damage. This component also considers the energy dissipation, G_c, attributed to the damage. The second component characterizes the stiffness degradation index, D, between the initial stage of damage and complete damage. The stiffness degradation index, D, is directly defined in terms of effective displacement and the relationship between effective displacement and damage. When adopting the linear displacement expansion criterion, the expression is

$$D = \frac{\delta_m^f \left(\delta_m^{max} - \delta_m^0\right)}{\delta_m^{max}\left(\delta_m^f - \delta_m^0\right)} \tag{5}$$

where δ_m^{max} is the maximum displacement of the cohesive unit undergoing damage, δ_m^f is the displacement in the cohesive unit during the fracture propagation and δ_m^0 is the displacement when the cohesive unit is transformed from the elastic phase to the destructive phase.

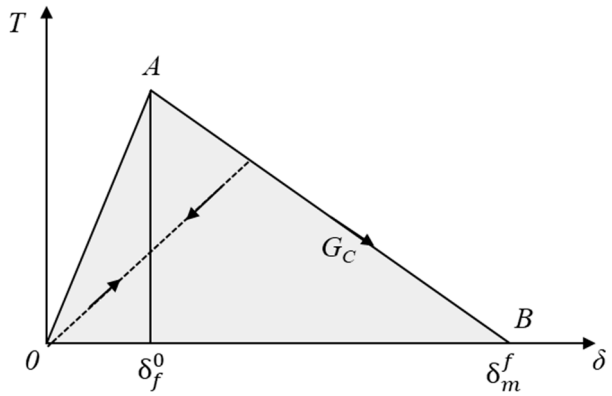

Figure 3. Cohesive linear-softening for the criterion.

The damage incurred by the rock can be quantified using the D. It is important to note that this condition is also valid when the rock sample is subjected to compressive stress. Therefore, the stiffness degradation criterion employed to characterize the fracture unit can be expressed as follows:

$$t_n = \begin{cases} (1-D)T_n, & T_n \geq 0 \\ T_n, & T_n < 0 \end{cases} \tag{6}$$

$$t_s = (1-D)T_s \tag{7}$$

$$t_t = (1-D)T_t \tag{8}$$

where T_n, T_s and T_t represent the stresses obtained from 3 directions.

The D depends on the softening nature of the rock in the reservoir.

$$\delta_m = \sqrt{\langle \delta_n \rangle^2 + \delta_s^2 + \delta_t^2} \tag{9}$$

where δ_m is the effective displacement obtained during the fracture propagation.

In this study, the B-K criterion is introduced to describe the fracture propagation.

$$G_n^c + (G_s^c - G_n^c)\left\{\frac{G_s + G_t}{G_s + G_t + G_n}\right\}^\eta = G^c \tag{10}$$

where G represents the energy release rate, n, s and t correspond to the 3 directions, and η represents a constant associated with the reservoir.

2.3. Fluid-Solid Coupling Equilibrium Equation

The upward normal leak-off of fluid along the fracture wall leads to an increase in pore pressure within the rock matrix surrounding the fracture. The effective stress in this context is influenced by both the rock skeleton and the pore pressure, p. The rise in pore pressure results in alterations in parameters such as reservoir porosity and fluid flow rate, subsequently impacting the normal fluid leak-off along the fracture wall [28].

In accordance with the principle of virtual work, the equilibrium equation can be expressed as follows:

$$\int_V (\overline{\boldsymbol{\sigma}} - p_w I)\delta\boldsymbol{\varepsilon} \mathrm{d}V = \int_S \boldsymbol{t} \cdot \delta\boldsymbol{v} \boldsymbol{d}S + \int_V f \cdot \delta\boldsymbol{v} \mathrm{d}V \tag{11}$$

where $\bar{\boldsymbol{\sigma}}$ and p_w are the Boit effective stress and pore pressure, respectively, $\delta_{\boldsymbol{\varepsilon}}$ and δ_v are the virtual strain rate and virtual velocity, respectively, and $\boldsymbol{t}$ and f are the surface displacement per unit area and body force per unit volume, respectively.

The change in fluid mass is equal to the mass of fluid flowing into and out of the cohesive surface per unit time.

$$\frac{1}{J}\frac{\partial}{\partial t}(J\rho_w n_w) + \frac{\partial}{\partial X}(\rho_w n_w v_w) = 0 \tag{12}$$

where J is the body variation ratio of reservoir rock, ρ_w is the fracturing fluid density in the fracture and n_w is the porosity.

Utilizing Darcy's law to describe the flow of fluid within the reservoir, the continuity equation for fluid leak-off can be expressed as follows:

$$v_w = -\frac{1}{n_w g \rho_w}\boldsymbol{k}\left(\frac{\partial p_w}{\partial x} - \rho_w g\right) \tag{13}$$

where $\boldsymbol{k}$ is the permeability of the reservoir.

2.4. Dynamic Distribution of Fluids

In hydraulic fracturing treatment, multiple fractures are usually formed when fracturing one or more sections of a well. As the formed hydraulic fractures squeeze the surrounding reservoir, stress shadows are formed, which can further influence the opening and propagation of the surrounding fractures. The flow pattern of the fracturing fluid in the wellbore and perforation cluster is shown in Figure 4. Due to the effect of wellbore friction, shot hole friction and resistance to fracture propagation, the amount of fluid intake during propagation of different hydraulic fractures in the same well is a dynamic equilibrium process. Similar to the shunt current in an electric circuit, the flow of fluid in each fracture needs to satisfy Kirchhoff's law [29].

$$Q = \sum_{1}^{N} Q_I \tag{14}$$

$$p_o = p_{pf,i} + p_{cf,i} + p_{w,i} \tag{15}$$

where Q is the total flow velocity in the wellbore, Q_i is the flow velocity into the ith fracture, p_o is the total pressure, p_{wi} is the pressure in the first unit in the ith fracture, $p_{cf,i}$ is the pressure loss in the horizontal wellbore and $p_{pf,i}$ is the pressure loss from shot hole.

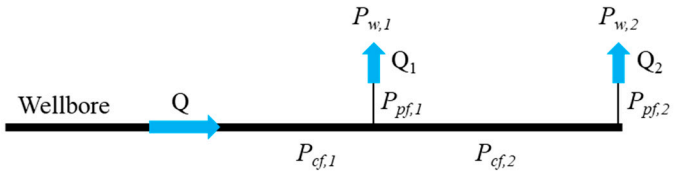

Figure 4. Dynamic distribution mode for fluid.

To address the issue of shot hole friction, a large number of researchers have shown that it is related to fluid properties, shot hole parameters, flow rate and other parameters. Among them, Crump [30] has established the relationship between shot hole resistance and fluid and shot hole parameters and flow rate based on a large number of experiments. This method is simple, efficient and highly integrated with Bernoulli's equation, and has been widely used by the industry.

$$\Delta p_{fric}^{I} = 0.807249\frac{\rho}{{n_p}^2 {D_p}^4 C^2} Q_I^2 \tag{16}$$

where Δp_{fric}^{I} is the pressure difference of perforation cluster I, Q_I is the flow velocity of perforation cluster I, n_p is the perforation number, D_p is the perforation diameter and C is the dimensionless coefficient characterizing the shape of perforation hole.

According to the calculation characteristics of perforation friction, the wellbore unit type is set to FP2D2, and the perforation unit type is set to FPC2D2 in the model. Because Churchill has the advantages of good convergence and wide application, this study uses it to calculate the perforation friction of perforation unit.

$$\Delta P - \rho g \Delta Z = K \frac{\rho Q^2}{2A^2} \tag{17}$$

where ΔP is the pressure difference, ΔZ is the elevation difference and K is the loss coefficient.

The values of K and A can be determined by combining Equations (16) and (17).

$$K = 2 \times 0.807249 \tag{18}$$

$$A = n_p \times C \times D_p^2 \tag{19}$$

2.5. Model Description

The schematic diagram of the model in this study is shown in Figure 5. Considering the size of fractures in hydraulic fracturing, the size of the model in this work is set to 160 m × 160 m, and one horizontal well is arranged at the upper and lower boundaries, respectively. There are one and two perforation clusters in wellbore 1 and wellbore 2 in the study area, respectively. Perforation cluster 1 (Perf 1) and perforation cluster 2 (Perf 2) satisfy the dynamic distribution of flow rate during the fracturing process. The injection rates of fracturing fluid in wellbore 1 and wellbore 2 are u_1 and u_2, respectively. The boundaries of the model are considered constant pressure boundaries. The initial pore pressure in the reservoir is denoted as P_b, and the minimum horizontal principal stress, maximum horizontal principal stress, and vertical stress are represented by S_h, S_H and S_v, respectively. The model employs the parameters listed in Table 1. The model was simulated using the software Abaqus, which has the CZM method embedded in it. Previous studies have demonstrated its good applicability for describing the hydraulic fracturing process [18,19]. It is worth noting that the stresses in all simulation results are effective stresses.

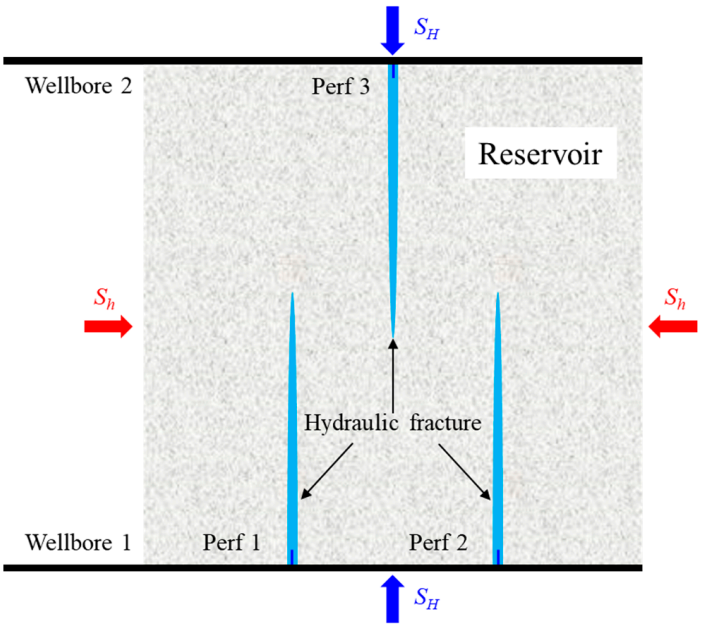

Figure 5. Schematic diagram of fracture propagation in the multi-horizontal well.

Table 1. The parameters used in this study.

Parameter	Value	Parameter	Value
S_h	65 MPa	Young's modulus	50 GPa
S_H	70 MPa	Poisson's ratio	0.25
S_v	75 MPa	Permeability	0.1 mD
P_b	48 MPa	Porosity	8.9%
Fluid viscosity	100 mPa·s	C	0.6
n_p	16	D_p	12 mm
Fluid density	1000 kg/m^3		

3. Result and Discussion

3.1. Mechanism of Inter-Well Interference

Fracture propagation can change the pore pressure and in situ stress in the reservoir, and clarifying the mechanism of inter-well fracture interference during fracturing is essential to optimize the effect of multi-well fracturing treatment. This section investigates fracture propagation and stress changes in two horizontal wells during the fracturing process. The spacing of the injection clusters in wellbore 1 is 60 m. The Young's modulus of the rock in the reservoir is 50 GPa. u_1 and u_2, the injection rate of the two wells, are 0.016 m/s and 0.008 m/s, respectively. The simulation results of the fracture propagation in the two wells during hydraulic fracturing are shown in Figure 6a. As can be seen from the figure, the fracture width of well 1 is smaller than that of well 2, but the fracture length of well 1 is larger than that of well 2. This is due to the fact that the fluid in the fracture needs to keep the fracture open during the fracture opening and propagation. The hydraulic fracture opening causes an increase in pressure on the rock around the fracture, resulting in an increase in the minimum principal stress in a certain area around the fracture (Figure 6b), which means the stress shadow is formed. The degree of this stress decreases gradually along the fracture propagation direction. Under the influence of the stress shadow, the maximum horizontal principal stress also shows the same trend (Figure 6c). Under the influence of the stress shadow generated by the adjacent fractures, the fractures in well 1 require more fluid pressure to maintain the fracture opening during the actual propagation (Figure 6d), and therefore the fracture width of the fractures formed in well 1 is smaller than that of the fractures formed in well 2. The smaller fracture width and larger fluid pressure allowed the fractures to propagate more rapidly because the fluid intake for each fracture was essentially the same in both wells. In summary, proper stress shade can increase the distance of fracture propagation.

The minimum horizontal principal stress is the key parameter to determine the fracture propagation, and the smaller the minimum horizontal principal stress is, the smaller the resistance to fracture opening and propagation. Figure 7 shows the distribution of the minimum horizontal principal stress at different stages of the fracture propagation process. As can be seen from the figure, the opening of the fracture in the reservoir will squeeze the rocks in the area around the fracture wall, thus increasing the minimum horizontal principal stress in the area. In the process of fracture propagation, the fracture tip will be tension damaged by the fracture fluid, and the rocks in the fracture tip area will be subjected to a certain degree of tension, thus making the minimum horizontal principal stress in the area decrease to different degrees. The fracture length in horizontal well 1 is shown in Figure 8. The fracture in horizontal well 1 is mainly influenced by its own intra-well interference at the early stage of propagation. After the fracture in well 1 propagates to the tension area formed by the fracture in horizontal well 2, the propagation rate of the hydraulic fracture in well 1 increases rapidly in this area because the minimum horizontal principal stress in this area decreases. With the continuous propagation of the fracture, when the hydraulic fracture of well 1 propagates to the compression area of well 2, the propagation rate of the fracture decreases rapidly at this time. As the fracture continues to propagate, the degree of decline is greater. There are two main reasons for this. One is that the closer to the root of the well 2 fracture, the greater the increase in the minimum horizontal principal stress in

the compression zone. The second is that as the fracture continues to propagate, the leak-off of fluid increases, and the propagation rate of the fracture itself gradually decreases.

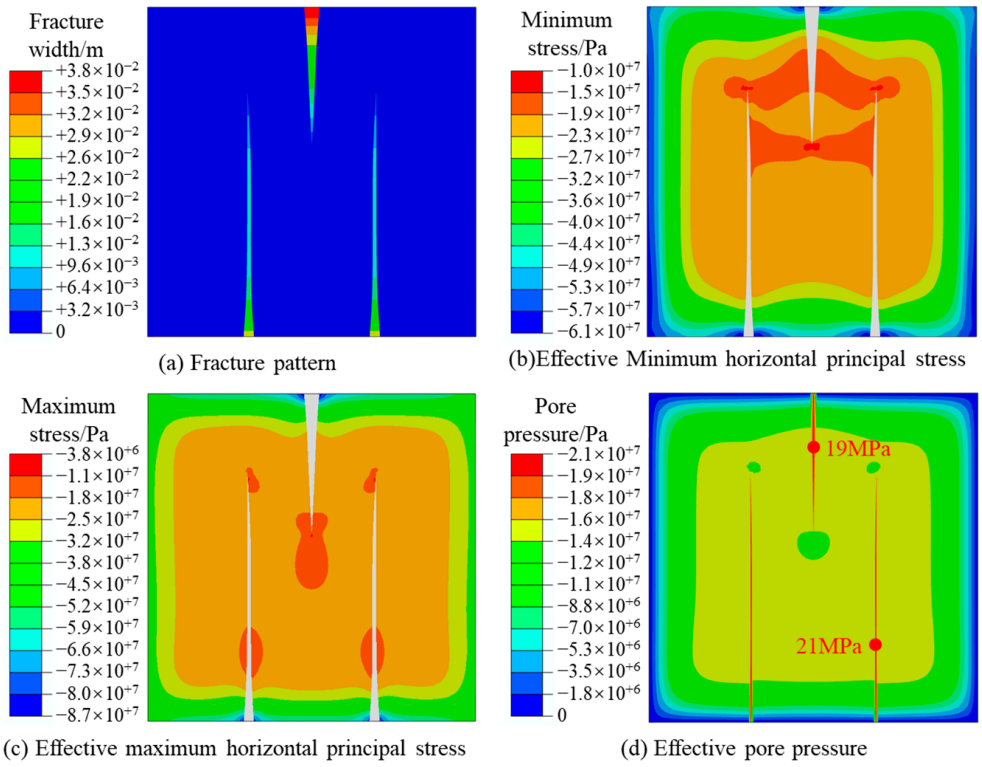

Figure 6. Fracture parameters and stress distribution during fracture propagation (150 s).

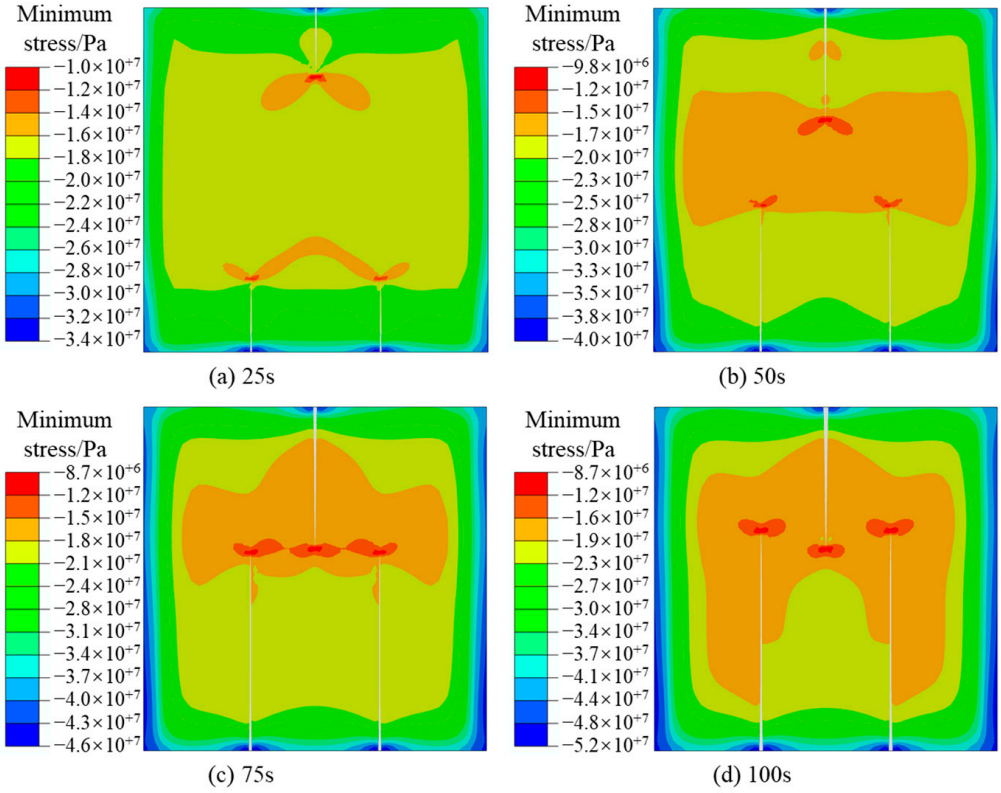

Figure 7. Distribution of the effective minimum horizontal principal stress during propagating.

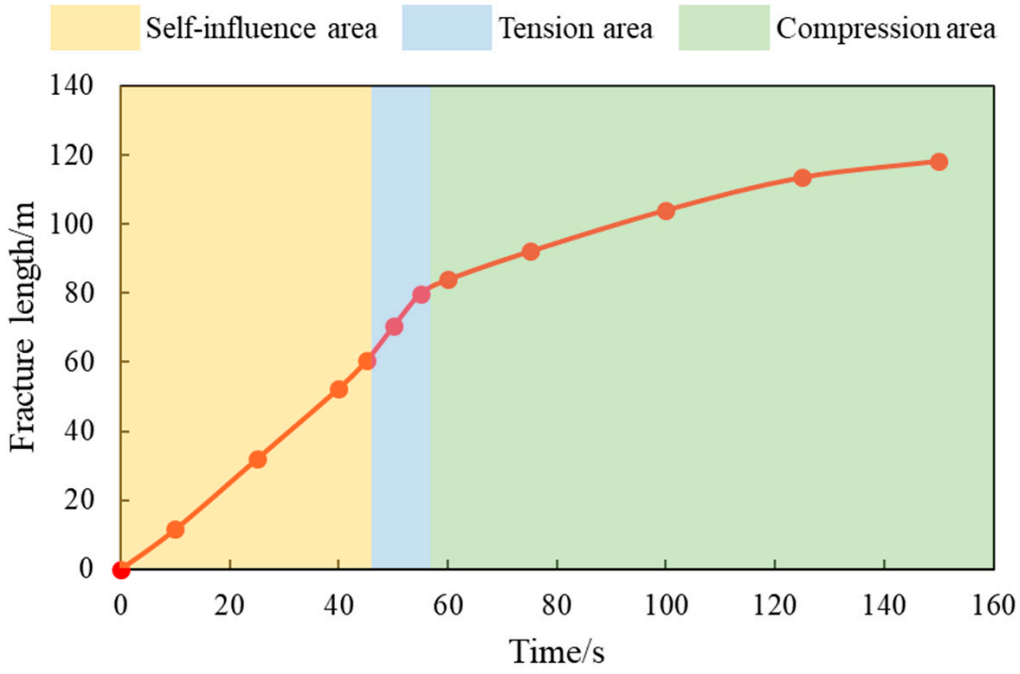

Figure 8. Hydraulic fracture length versus time in horizontal well 1.

3.2. Effect of Young's Modulus

The fracturing fluid enters the reservoir along the wellbore from the perforation cluster, and the high-pressure fluid opens the reservoir to form a fracture. The fluid in the fracture squeezes the rock around the fracture wall and causes deformation. Young's modulus is an important parameter for quantitatively evaluating the stress–strain relationship of rocks. In this section, the propagation pattern of the fracture is studied for Young's modulus of the reservoir rock at 30 GPa, 40 GPa, 50 GPa and 60 GPa, respectively, and the simulation results are shown in Figures 9 and 10. From the figures, it can be seen that with the increasing Young's modulus, the fracture width shows a decreasing trend, but the fracture length shows an increasing trend. Among them, the maximum fracture widths of Perf 1 are 3.12 cm, 2.70 cm, 2.49 cm and 2.34 cm, respectively. The maximum fracture widths of Perf 3 are 3.82 cm, 3.58 cm, 3.55 cm and 3.54 cm, respectively. The fracture lengths of Perf 1 are 80.54 m, 103.24 m, 113.76 m and 124.02 m, respectively. The maximum fracture lengths of Perf 3 are 60 m, 63.51 m, 63.89 m and 65.29 m. It is worth noting that proper intra-well interference can increase the stimulation pressure and reduce the fracture width, which can enhance the fracture propagation distance under a constant pumping rate in the field [16]. Rocks with lower Young's modulus tend to be more plastic and form hydraulic fractures with typically shorter fracture lengths and larger fracture widths [25]. The fracture width in well 1 is further reduced compared to that in well 2 due to stress shade, resulting in a hydraulic fracture more sensitive to Young's modulus in well 1. In addition, combined with the relative positions of the fractures between wells in Figure 10, it can be seen that with the increase in Young's modulus, the fractures will propagate to the tension area more quickly, and the existence of the tension area will further increase the distance of fracture propagation. When the fracture continues to propagate to the compression area, the propagation rate of the fracture will decrease. In summary, the fracture length and width of multi-horizontal wells are controlled by both Young's modulus and inter-well interference.

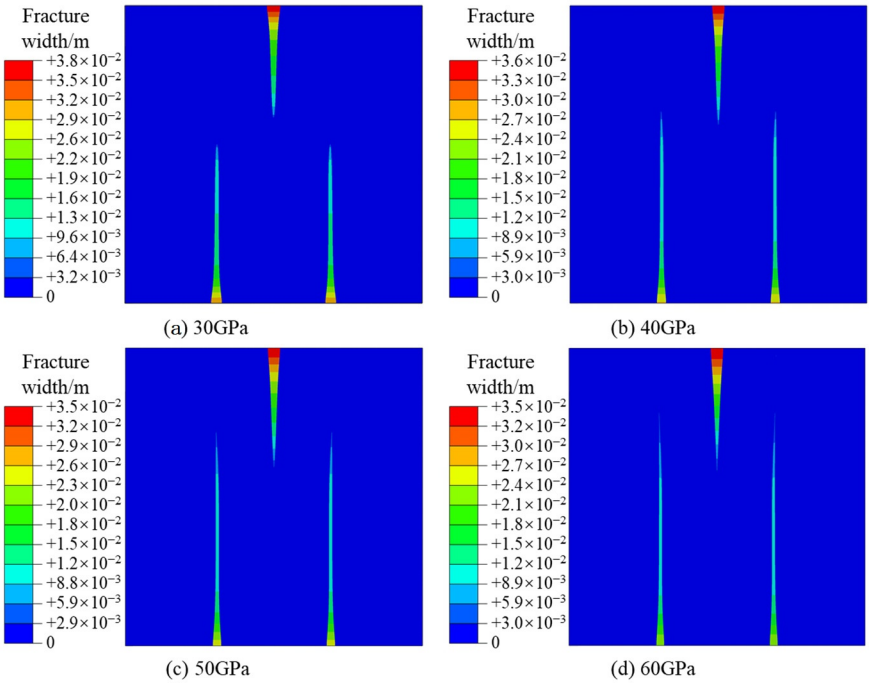

Figure 9. Fracture width of hydraulic fractures at different Young's modulus (140 s).

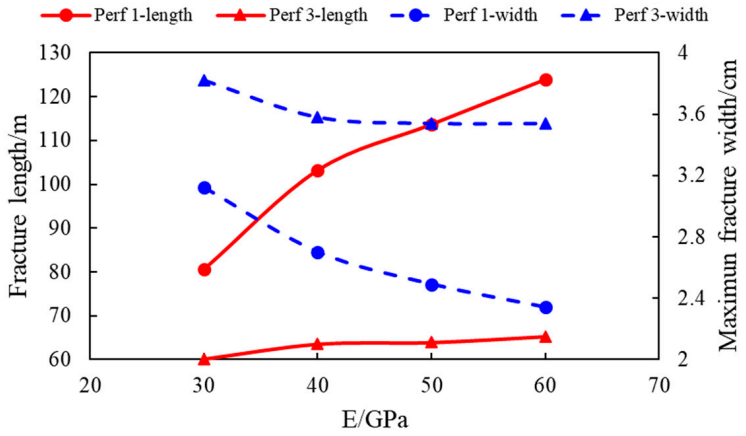

Figure 10. Fracture length and maximum fracture width at different Young's modulus.

3.3. Effect of Fracture Placement Location

In hydraulic fracturing stimulation, the relative position of the perforation clusters in the wellbore is often not uniformly distributed. Under the combined influence of geological and engineering factors, the distance between perforation clusters usually varies. Due to fracturing interference between multi-horizontal wells, the relative position of the perforation clusters between wells is an important factor affecting fracture propagation. This section investigates the fracture propagation results for the lateral distances of Perf 3 to Perf 1 and Perf 2 at 30 m and 30 m (30 m–30 m), 20 m–40 m and 10 m–50 m, respectively. In order to more intuitively reflect the influence of the location of the fractures, we chose the fracture propagation results after 100 s of fluid injection (Figure 11) as the object of comparison. From the fracture propagation results, it can be seen that the formed hydraulic fracture has an inhibitory effect on the propagation of the closer fracture in the neighboring wells, and this inhibitory effect gradually increases as the distance decreases. In the case of 10 m–50 m, the lengths of Perf 1 and Perf 2 are 128.7 m and 36.9 m, respectively. In the case of 30 m–30 m, 20 m–40 m and 10 m–50 m fracture placement patterns, the ratio of the fracture lengths of Perf 2 and Perf 1 have fracture length ratios of 1, 1.76 and 3.49, respectively.

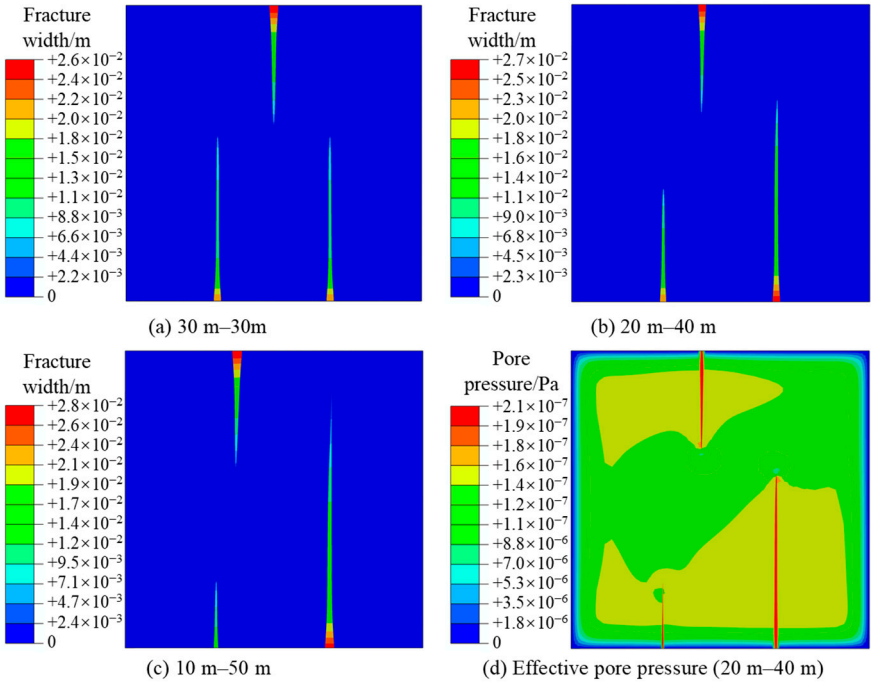

Figure 11. The propagation state of hydraulic fractures at different placement positions (100 s).

It is clear from the distribution of pore pressure that the formation of the dominant fracture (Perf 2) due to the difference in interference caused by the placement pattern will in turn force the flow of fluids from the neighboring well fracture (Perf 3) to the other side, thus further inhibiting the propagation process of the inferior fracture (Perf 1). Due to the difference in propagation resistance, the fluid intake of the perforation clusters in a well is a dynamic distribution process, and the relationship between the flow rates of Perf 1 and Perf 2 during fracture propagation is shown in Figure 12. As can be seen from the figure, at the early stage of propagation, the interference between wells is small, and at this time the perforation clusters have the same flow distribution ratio among them. As the fracture continues to propagate, the gradually increasing inter-well interference makes Perf 1 become the inferior fracture and Perf 2, which becomes the dominant fracture, receives more fluid. As Perf 1 continues to feed fluid, the interference from Perf 1 to Perf 2 gradually increases, causing the amount of fluid fed to Perf 2 to decrease slightly. When Perf 2 propagates into the tension area of the neighboring well fracture, the fluid feed at this point shows a brief increase. After finally entering the compression area, the fluid volume of Perf 1 and Perf 2 gradually stabilizes.

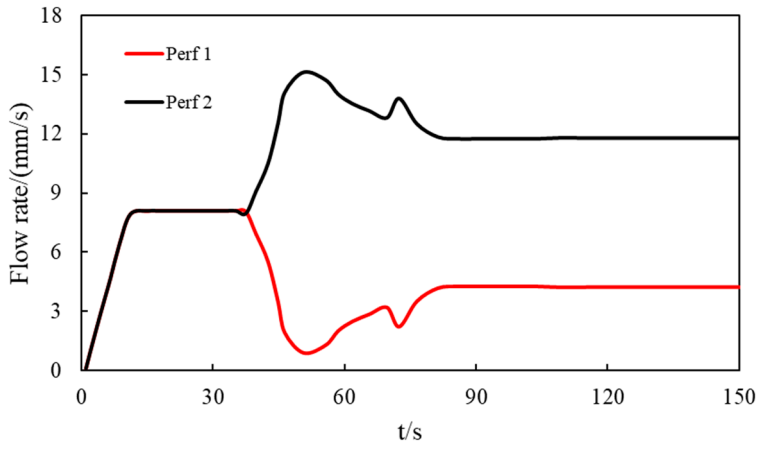

Figure 12. Dynamic distribution of flow rates in Perf 1 and Perf 2 for the case of 10 m–50 m.

4. Conclusions

In this study, the coupled model of fluid flow and solid damage and deformation is constructed by using the bilinear T-S criterion and the stiffness degradation to describe the damage and evolution of fractures, and the dynamic distribution of fluid due to uneven fracture propagation in the hydraulic fracturing is realized based on the CZM finite element model. The main conclusions are obtained as follows.

(1) Stress shade of multiple fractures can reduce the fracture width while increasing the fracture length. According to the stress distribution state in the hydraulic fracture propagation in multi-horizontal wells, the reservoir can be divided into the self-influence area, tension area and compression area. The propagation rate of the hydraulic fractures in horizontal wells accelerates significantly when they propagate to the local tension area generated by the fracture tip of neighboring wells and decreases rapidly as the hydraulic fractures continue to propagate to the compression area of neighboring wells.

(2) Proper intra-well interference can increase the fracture propagation distance. Reservoirs with higher Young's modulus are usually more brittle, and the fracture width and fracture length formed during hydraulic fracturing are smaller and longer, respectively.

(3) Hydraulic fractures have an inhibitory effect on the propagation of closer fractures in neighboring wells, and this inhibitory effect gradually increases as the distance decreases. The formation of the dominant fracture will further influence the pore pressure field, thus inhibiting the propagation of the inferior fracture in the same well. The dominance of the dominant fracture to propagate in the self-influence area gradually decreases under inter-well and intra-well interference. As the dominant fracture propagates into the tension and compression areas of the neighboring well fractures, the feed fluid will show a brief rise and then eventually stabilize.

In this study, the effect of the stress shadow on fracture propagation during the fracturing process of multi-horizontal wells is studied more systematically. However, the reservoir permeability of 0.1 mD in the model does not consider the effect of pore elasticity on fracture propagation during hydraulic fracturing. The coupling of fluid and pore elasticity deformation on fracture propagation in multi-horizontal wells hydraulic fracturing still needs to be studied continuously.

Author Contributions: Writing-Original manuscript, Q.R.; supervision, X.Z.; investigation, J.D.; data curation, M.X.; formal analysis, D.R. and R.L. All authors have read and agreed to the published version of the manuscript.

Funding: This research was funded by the Key Core Technology Research Projects of PetroChina Company Limited (No. 2020B-4911) and the APC was funded by the Research Institute of Petroleum Exploration and Development.

Data Availability Statement: No new data were created or analyzed in this study. Data sharing is not applicable to this article.

Conflicts of Interest: The authors declare no conflict of interest.

References

1. Wang, Y.; Zhou, F.; Zhang, Y.; Wang, Y.; Su, H.; Dong, R.; Wang, Q.; Bai, H. Numerical studies and analysis on reaction characteristics of limestone and dolomite in carbonate matrix acidizing. *Geoenergy Sci. Eng.* **2023**, *222*, 211452. [CrossRef]
2. Li, M.; Zhou, F. Multi-fracture initiation sequence and breakdown pressure in horizontal wells during TDPF: A visualization experimental investigation based on PMMA. *J. Pet. Sci. Eng.* **2022**, *215*, 110645. [CrossRef]
3. Wu, K.; Olson, J.E. Mechanisms of Simultaneous Hydraulic-Fracture Propagation from Multiple Perforation Clusters in Horizontal Wells. *SPE J.* **2016**, *21*, 1000–1008. [CrossRef]
4. Huang, W.; Kamenski, L. A geometric discretization and a simple implementation for variational mesh generation and adaptation. *J. Comput. Phys.* **2015**, *301*, 322–337. [CrossRef]
5. Chu, H.; Chen, Z.; Liao, X.; Lee, W.J. Transient behavior modeling of a multi-well horizontal pad in a reservoir with irregular boundary using boundary element method. *J. Pet. Sci. Eng.* **2022**, *209*, 109852. [CrossRef]

6. Seth, P.; Manchanda, R.; Kumar, A.; Sharma, M.M. Analyzing Pressure Interference between Horizontal Wells during Fracturing. *J. Pet. Sci. Eng.* **2021**, *204*, 108696. [CrossRef]
7. Dong, R.; Wheeler, M.F.; Ma, K.; Su, H. A 3D Acid Transport Model for Acid Fracturing Treatments with Viscous Fingering. Presented at the SPE Annual Technical Conference and Exhibition, Virtual, 26–29 October 2020. [CrossRef]
8. Dong, R.; Wheeler, M.F.; Su, H.; Ma, K. Modeling Multistage Acid Fracturing Treatments in Carbonate Reservoirs. Presented at the SPE Hydraulic Fracturing Technology Conference and Exhibition, Virtual, 4–6 May 2021. [CrossRef]
9. Carrier, B.; Granet, S. Numerical modeling of hydraulic fracture problem in permeable medium using cohesive zone model. *Eng. Fract. Mech.* **2012**, *79*, 312–328. [CrossRef]
10. Sarris, E.; Papanastasiou, P. The influence of the cohesive process zone in hydraulic fracturing modelling. *Int. J. Fract.* **2011**, *167*, 33–45. [CrossRef]
11. Dong, R.; Alpak, F.O.; Wheeler, M.F. Accurate Two-Phase Flow Simulation in Faulted Reservoirs by Combining Two-Point Flux Approximation and Mimetic Finite Difference Methods. *SPE J.* **2023**, *28*, 111–129. [CrossRef]
12. Lin, H.; Deng, J.; Liu, W.; Xie, T.; Xu, J.; Liu, H. Numerical simulation of hydraulic fracture propagation in weakly consolidated sandstone reservoirs. *J. Cent. South Univ.* **2018**, *25*, 2944–2952. [CrossRef]
13. Guo, J.; Zhao, X.; Zhu, H.; Zhang, X.; Pan, R. Numerical simulation of interaction of hydraulic fracture and natural fracture based on the cohesive zone finite element method. *J. Nat. Gas Sci. Eng.* **2015**, *25*, 180–188. [CrossRef]
14. Li, Y.; Deng, J.G.; Liu, W.; Feng, Y. Modeling hydraulic fracture propagation using cohesive zone model equipped with frictional contact capability. *Comput. Geotech.* **2017**, *91*, 58–70. [CrossRef]
15. Zou, J.; Zhang, Y.; Zhang, L.; Jing, J.; Fu, Y.; Wang, Y.; Zhang, G.; Zhou, F. Numerical Simulation Research on the Effect of Artificial Barrier Properties on Fracture Height. *Processes* **2023**, *11*, 310. [CrossRef]
16. Zhu, D.; Wang, Y.; Cui, M.; Zhou, F.; Wang, Y.; Liang, C.; Zou, H.; Yao, F. Acid System and Stimulation Efficiency of Multistage Acid Fracturing in Porous Carbonate Reservoirs. *Processes* **2022**, *10*, 1883. [CrossRef]
17. Li, J.; Dong, S.; Hua, W.; Li, X.; Pan, X. Numerical Investigation of Hydraulic Fracture Propagation Based on Cohesive Zone Model in Naturally Fractured Formations. *Processes* **2019**, *7*, 28. [CrossRef]
18. Lecampion, B. An extended finite element method for hydraulic fracture problems. *Commun. Numer. Methods Eng.* **2009**, *25*, 121–133. [CrossRef]
19. Chen, Z.; Bunger, A.P.; Zhang, X.; Jeffrey, R.G. Cohesive Zone Finite Element-Based Modeling of Hydraulic Fractures. *Acta Mech. Solida Sin.* **2009**, *22*, 443–452. [CrossRef]
20. Wu, B.; Zhang, M.; Deng, W.; Que, J.; Liu, W.; Zhou, F.; Wang, Q.; Li, Y.; Liang, T. Study and Mechanism Analysis on Dynamic Shrinkage of Bottom Sediments in Salt Cavern Gas Storage. *Processes* **2022**, *10*, 1511. [CrossRef]
21. Yuan, K.; Huang, W.; Chen, X.; Cao, Q.; Fang, X.; Lin, T.; Jin, C.; Li, S.; Wang, C.; Wang, T. The Whole-Aperture Pore Structure Characteristics and Their Controlling Factors of the Dawuba Formation Shale in Western Guizhou. *Processes* **2022**, *10*, 622. [CrossRef]
22. Sun, S.; Zhou, M.; Lu, W.; Davarpanah, A. Application of Symmetry Law in Numerical Modeling of Hydraulic Fracturing by Finite Element Method. *Symmetry* **2020**, *12*, 1122. [CrossRef]
23. Zhu, D.; Wang, Y.; Cui, M.; Zhou, F.; Zhang, Y.; Liang, C.; Zou, H.; Yao, F. Effects of spent viscoelastic-surfactant acid flow on wormholes propagation and diverting performance in heterogeneous carbonate reservoir. *Energy Rep.* **2022**, *8*, 8321–8332. [CrossRef]
24. Zhu, H.; Wang, H.; Tang, X.; Li, Y. Hydraulic Fracture Propagation in Sand-Mudstone Interbedded Reservoir Integrated with Different Fluid Flow of Multi-Perforated Fractures. Presented at the ARMA-CUPB Geothermal International Conference, Beijing, China, 5–8 August 2019. Available online: https://onepetro.org/ARMACUPB/proceedings-abstract/CUPB19/All-CUPB19/125225 (accessed on 17 March 2023).
25. Peng, Y.; Zhao, J.; Sepehrnoori, K.; Li, Z. Fractional model for simulating the viscoelastic behavior of artificial fracture in shale gas. *Eng. Fract. Mech.* **2020**, *228*, 106892. [CrossRef]
26. Biot, M.A. General Theory of Three-Dimensional Consolidation. *J. Appl. Phys.* **1941**, *12*, 155–164. [CrossRef]
27. Tomar, V.; Zhai, J.; Zhou, M. Bounds for element size in a variable stiffness cohesive finite element. *Int. J. Numer. Methods Eng.* **2004**, *61*, 1894–1920. [CrossRef]
28. Peng, Y.; Zhao, J.; Sepehrnoori, K.; Li, Z.; Xu, F. Study of delayed creep fracture initiation and propagation based on semi-analytical fractional model. *Appl. Math. Model.* **2019**, *72*, 700–715. [CrossRef]
29. Elbel, J.L.; Piggott, A.R.; Mack, M.G. Numerical Modeling of Multilayer Fracture Treatments. Presented at the Permian Basin Oil and Gas Recovery Conference, Midland, TX, USA, 18–20 March 1992. [CrossRef]
30. Crump, J.B.; Conway, M.W. Effects of Perforation-Entry Friction on Bottomhole Treating Analysis. *J. Pet. Technol.* **1988**, *40*, 1041–1048. [CrossRef]